Received: 21 July 2022 | Revised: 20 September 2022 | Accepted: 24 September 2022

DOI: 10.1002/aoc.6930

RESEARCH ARTICLE

Applied Organometallic Chemistry WILEY

One-dimensional metal–organic frameworks built by coordinating 2,4,6-tris(4-pyridyl)-1,3,5-triazine linker with copper nodes: CO_2 adsorption properties

Núria Portolés-Gil[1] | **Oriol Vallcorba**[2] | **Julio Fraile-Sainz**[1] | **Ana M. López-Periago**[1] | **Concepción Domingo**[1] | **José A. Ayllón**[3]

[1]Instituto de Ciencia de Materiales de Barcelona, CSIC, Campus UAB, Bellaterra, Spain

[2]ALBA Synchrotron Light Source, CELLS, Barcelona, Spain

[3]Department of Chemistry, Universitat Autònoma de Barcelona, UAB, Bellaterra, Spain

Correspondence
José A. Ayllón, Department of Chemistry, Universitat Autònoma de Barcelona, UAB, 08193 Bellaterra, Spain.
Email: joseantonio.ayllon@uab.cat

Funding information
Spanish Ministry of Science and Innovation (MICINN), Grant/Award Number: CEX2019-000917-S; Spanish National Plan of Research, Grant/Award Number: PID2020-115631GB-I00

The reaction between 2,4,6-tris(4-pyridyl)-1,3,5-triazine (4-tpt) and copper(II) hexafluoroacetylacetone ($Cu(hfa)_2$) yields two different 1D metal–organic frameworks (MOFs), $[(Cu(hfa)_2)_2(4\text{-tpt})]_n$ (**1**) and $[Cu(hfa)_2(4\text{-tpt})]_n$ (**2**). The Cu:4-tpt ratio in the new MOFs is determined by the reaction medium, particularly, the solvent used. The two compounds have been fully characterized, including crystal structure elucidation. $[(Cu(hfa)_2)_2(4\text{-tpt})]_n$ (**1**), with a 2:1 Cu:4-tpt ratio, could be precipitated in either 1,1,2-trichloroethane or supercritical CO_2. In (**1**), 4-tpt shows a tritopic coordination mode, but only half of the $Cu(hfa)_2$ subunits act as a node, thus connecting two 4-tpt and giving a 1D network. The other half of $Cu(hfa)_2$ subunits are connected only to one pyridine and thus protrude along the chains. The later $Cu(hfa)_2$ fragments show a labile character and can be dissolved in diethyl ether to give the second MOF $[Cu(hfa)_2(4\text{-tpt})]_n$ (**2**), with a 1:1 Cu:4-tpt ratio. The compound (**2**) has also a 1D structure, with all the incorporated copper atoms acting as nodes. In this case, the packing of the chains defines accessible channels, which are perpendicular to the chain axis. After activation, N_2 adsorption/desorption measurements at 77 K confirm the microporous character of (**2**) with an apparent surface area of 190 $m^2\ g^{-1}$. Besides, at 273 K this material clearly shows a significant adsorption of CO_2 prompted by noncoordinated nitrogen in the triazine linker.

KEYWORDS
CO_2 adsorption, metal–organic framework, solid-phase transformation, triazine, tritopic linker

1 | INTRODUCTION

In the actual technological scenario, processes involving gasses, as those related to energy, transport, chemical synthesis, separation, or purification, among others, are of enormous importance, which, presumably, would increase in the near future. In this context, the design and fabrication of porous materials that facilitates the manipulation and storage of these gasses is necessary to improve future applications.[1] This need has promoted

the development of new porous materials, among which stands out the family of metal–organic frameworks (MOFs), with huge compositional tunability achieved by the proper combination of metallic nodes and organic linkers that can yield a material with the desired properties.[2] Hence, MOFs are considered emergent options to replace traditional porous materials, such as zeolites or porous carbons, in most applications.

2,4,6-Tris(4-pyridyl)-1,3,5-triazine (4-tpt) is a ligand specially interesting for the design of new MOFs. It is essentially planar and rigid, exhibiting a potential tritopic coordination mode, although structures with 4-tpt acting as a ditopic linker are often found.[3] 4-tpt is most versatile than other 2,4,6-tris(pyridyl)-1,3,5-triazine isomers, because the three pyridyl groups are equally accessible for complexation.[4] Consequently, 4-tpt has been extensively exploited in coordination chemistry coupled to transition metals and lanthanides[3,5] and has already afforded several unusual and highly symmetrical MOFs.[6–13] For instance, it is remarkable the design of the $[(ZnI_2)_3(4\text{-tpt})_2]_n$ as a crystalline sponge, a subset of MOFs that have been tailored to enhance crystallographic investigations by providing a cavity capable of ordering guest molecules.[14] The ordering of these substances inside the MOF pores has allowed the determination of the structure of compounds available in only very small amounts (nanograms) or difficult to crystalize.[15,16]

Regarding the use of 4-tpt to produce porous materials, additional benefits arise from the weak basicity of the triazine central ring, which do not usually coordinate to metal centers, and, thus, it is available to interact with acid adsorbates in sorption applications.[17–20] This is considered as a key advantage, because most Lewis basic sites tend to be involved in coordination bonds with metal ions and thus are withdrawn for adsorption. The triazine basicity properties have been used to achieve in particular coordination networks of an improved adsorption for different gaseous molecules, such as CO_2 and CH_4.[21] The neutral 4-tpt linker can be combined with noncharged nodes to produce neutral coordination polymers (CPs) and MOFs with chelated units, which are an interesting topic in the branch of coordination chemistry due to their specific properties.[22] In our past research, several MOFs were obtained in our laboratories from the combination of metal(II) hexafluoroacetylacetone ($M(hfa)_2$) complexes (M = Cu, Zn, Co) with different ditopic and tritopic pyridines.[23–25] Particularly, the characteristic high solubility of $Cu(hfa)_2$ in a large variety of solvents used for the synthesis of CPs and MOFs, including supercritical CO_2 ($scCO_2$), encouraged its regular use as a metal node in these structures. Actually, most of the described CPs and MOFs based on the 4-tpt linker have been hydrothermally synthesized.[26] In contrast, the focus of this work is in the design of synthetic processes that avoid the use of hydrothermal techniques and high boiling point solvents.

It has been established that modifications in the reaction conditions, and, especially, in the solvent, determines the structure of the framework formed from a determined set of precursors. This general observation also applied to the synthesis of solids involving triazines. For example, the analysis of a 4-tpt closely related linker, the 3-tpt (2,4,6-tris(3-pyridyl)-1,3,5-triazine), determines the existence various coordination modes for it, bidentate and tridentate, resulting in a series of 1D or 2D polymeric structures after reaction with $[Cu(hfa)_2]$. The polarity of the solvent determines the 3-tpt symmetric or asymmetric conformation.[25] In contrast to 3-tpt, the 4-tpt linker can only stand the symmetric conformation. In this case, the solvent polarity would not influence the molecular conformation of the reacting linker, because only one is available in all the different situations. However, it has been observed that even under these circumstances of tritopic symmetric linkers, the choice of solvent can be used to determine the precipitated structure. Only few examples of the solvent influence have previously been reported in the synthesis of 4-tpt derivatives, focused on the use of iron thiocyanate, giving compounds with different Fe:4-tpt ratio.[27] On this basis, the main objective in this study was to extend the study of the solvent influence for the manipulation of 4-tpt MOF structures, distinctively those involving Cu(II) as the metal node. It is demonstrated that the solvent used in the synthesis can determine the denticity (tritopic or ditopic) of the 4-tpt in their combination with $[Cu(hfa)_2]$. The two new obtained compounds, $[(Cu(hfa)_2)_2(4\text{-tpt})]_n$ (**1**) and $[(Cu(hfa)_2)(4\text{-tpt})]_n$ (**2**), where fully characterized, including crystal structure determination. In regard of applications, the significant adsorption of CO_2 prompted by noncoordinated nitrogen in the triazine linker was established.

2 | RESULTS AND DISCUSSION

2.1 | Synthesis

Two different MOFs, with a different Cu:4-tpt ratio and crystalline structure, where precipitated in this work: $[(Cu(hfa)_2)_2(4\text{-tpt})]_n$ (**1**) and $[(Cu(hfa)_2)(4\text{-tpt})]_n$ (**2**). Compound (**1**), with a 2:1 Cu:4-tpt ratio, was straightforwardly precipitated from a mixture of the reagents dissolved in either hot trichloroethane (TCE) (353 K) or in $scCO_2$ (333 K). On the contrary, compound (**2**), with a 1:1 Cu:4-tpt ratio, must be precipitated by recrystallization in EtOEt of an intermediate phase consisting in either an amorphous solid obtained in $CHCl_3$ or the

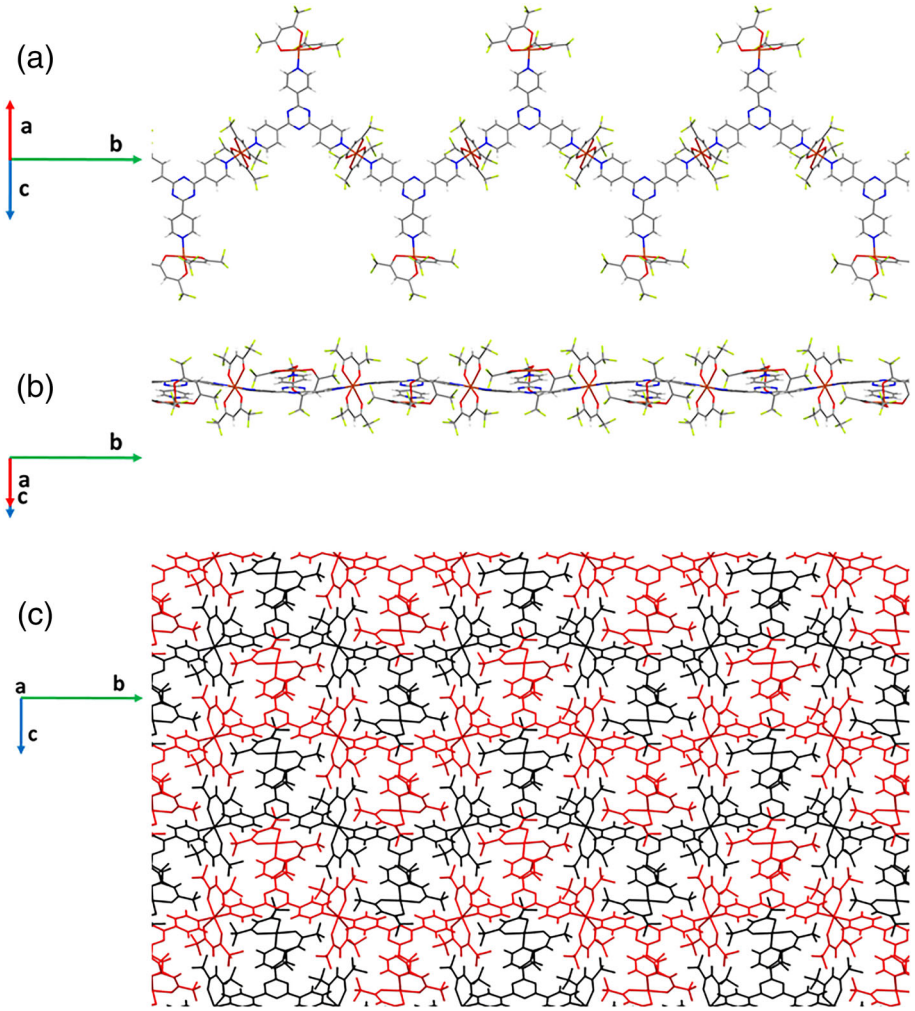

FIGURE 1 Crystal structure of $[(Cu(hfa)_2)_2(4\text{-tpt})]_n$ (**1**): (a,b) views of the chains with a different angle in respect to the 4-tpt linker and (c) packing in which all the chains are equivalent (neighbor chains are differently colored in red and black to facilitate the understanding)

crystalline compound (**1**). The structure of these compounds is described in the next section.

2.2 | Structures

2.2.1 | Structure of (**1**)

Compound $[(Cu(hfa)_2)_2(4\text{-tpt})]_n$ (**1**) crystallizes in the monoclinic P 2_1 space group. The unit cell parameters are $a = 10.5172(2)$ Å, $b = 25.4118(4)$ Å, and $c = 10.0730(2)$ Å, with $\beta = 112.974(1)°$ (see Table S1 for additional structural information). The asymmetric unit includes two $Cu(hfa)_2$ fragments and one 4-tpt linker. Although 4-tpt acts as a tritopic ligand, only half of the Cu(II) atoms connect two 4-tpt linkers, placed at relative *trans* positions. This distribution of linkers and metal nodes results in a 1D MOF (Figure 1a,b). The Cu(II) atoms in this node, Cu1a, present a distorted octahedral coordination, encompassing four oxygen on the equatorial plane and two nitrogen at axial positions. One of the Cu—O distances, Cu1a—O1a (2.34 Å), is noticeably larger than the other three (1.92–2.10 Å) (Figure S1), depicting an asymmetric coordination of hfa to Cu, which has been previously reported in a comparable coordination environment.[28–31] The propagation of the Cu1a—N6c and Cu1a—N14c bonds, which involves two of the three pyridinic nitrogen atoms of each 4-tpt linker, defines chains parallel to the ***b*** direction. The remaining pyridine groups are attached to the other independent $Cu(hfa)_2$ fragments, yielding thus a pentacoordinated Cu(II) center, Cu1b, which presents a distorted square-base pyramid coordination, with the nitrogen and three oxygen atoms defining the base, and the remaining oxygen located at the apex (Figure S1). In these subunits, one of the main planes defined by one CCCOCuO ring (metal and one hfa) is almost perpendicular to the pyridine ring (88.55°), while the other is only lightly tilted with regards to the plane of the pyridine ring (14.64°). Although the pyridine adducts of $Cu(hfa)_2$ are most frequently hexacoordinated, each Cu(II) atom being usually bonded to two pyridine groups, few examples are also

known in which each copper is linked to only one nitrogen yielding pentacoordinated Cu(II) centers.[29,32] It is also noticeable that, in the coordination sphere of Cu1b, all the ligands are positioned in a hemisphere. This arrangement favors a weak interchain interaction between the Cu(II) and one of the nitrogen atoms of the central triazine ring of a 4-tpt ligand (Figure S2). 4-tpt linker deviates from planarity, showing a slightly concave shape, in which two of the pyridine rings are slanted with regards to the central triazine ring plane (16–18°). The packing of the chains involves, besides the Cu···N contact previously mentioned, weak intermolecular F···F and C_{ar}-H···F contacts, yielding a supramolecular compact packing (Figure 1c). The crystal structure of $[(Cu(hfa)_2)_2(4\text{-tpt})]_n$ resembles the recently reported one for $[(Cu(hfa)_2)_2(3\text{-tpt})]_n$, although the 3-tpt compound was only obtained in trace amounts as it evolves to the formation of $[(Cu(hfa)_2)_{1.5}(3\text{-tpt})]_n \cdot 3H_2O$ as the predominant compound, in which all the Cu(II) atoms are linked to two pyridine groups.[25] Likely, the system with 4-tpt cannot progress to a polymer of similar stoichiometry due to the less flexibility of this linker with respect to 3-tpt.

2.2.2 | Structure of (2)

Compound $[(Cu(hfa)_2)(4\text{-tpt})]_n$ (**2**) crystallizes in the monoclinic $P2_12_12$ space group. The unit cell parameters are $a = 20.009(9)$ Å, $b = 26.391(3)$ Å, and $c = 6.3860(3)$ Å (see Table S2 for additional structural information). The asymmetric unit includes one $Cu(hfa)_2$ fragment and one 4-tpt linker. The Cu(II) centers, showing distorting octahedral coordination, constitute connection knots through pyridine groups coordination from two 4-tpt (N-Cu-N angle: 178.8(2)°), while the equatorial positions are occupied by the oxygen atoms from the two chelating hfa ligands (Cu—O distances in the 2.091–2.098 Å range) (Figure S3). 4-tpt is here acting as a ditopic ligand, bridging pairs of metals through two of its pyridyl moieties. This conformation defines 1D zigzag chains, parallel to the [010] direction (Figure 2a,b). A similar chain has been described for a MOF involving $Cu(hfa)_2$ and dibenzoyl chelating instead of hfa.[5] The 4-tpt linker deviates from planarity, showing a slightly concave shape, but in a less pronounced fashion than in (**1**). In (**2**), two of the pyridine rings are also slanted regarding the central triazine ring plane, but with lower angles (8° to 10°) than those observed in (**1**). The interchain interaction in (**2**) includes an asymmetric π–π contact between the noncoordinated pyridine in the ring and the central triazine ring of neighbor chains (Figure S4). The centroid–centroid distance is 3.535 Å, although two C—C distances are noticeable shorter, around 3.27 Å. The packing of the chains involves the Cu···N contact previously mentioned in (**1**), as well as the other weak intermolecular F···F and C_{ar}-H···O interactions. In this case, the packing of the chains defines channels parallel to the ***c*** axis, which contain residual water molecules. The channels have an elongated section and narrow periodically (Figures 2c,d and S5).

2.3 | Solvent influence

As for many other coordination compounds, the crystallization experimental parameters, particularly the used solvent, are critical to determine the different coordination networks that can be produced from the combination of the 4-tpt linker and the $[Cu(hfa)_2]$ complex. This study was initially performed analyzing the system 4-tpt/$Cu(hfa)_2$ in a large number of solvents different from water, such as 1,1,2-TCE, chloroform ($CHCl_3$), $scCO_2$, diethyl ether (EtOEt), ethanol, tetrahydrofuran, methoxyethanol, and mixtures, such as hexafluoroisopropanol and chloroform. Most of these solvents produced amorphous compounds. Because it was not possible to characterize the complete spectrum of materials, solvents leading to porous compounds with potentially adsorption applications were chosen for analysis in this work. Precipitation experiments were carried out in solvents in which at least one of the two regents was soluble (EtOEt, $scCO_2$), or even both were soluble (hot TCE, $CHCl_3$).

As mentioned previously, compound (**1**) can be simply precipitated from a solution involving the reagents in the proper ratio. TCE, a solvent that allows the use of high working temperatures in nonpressurized vessels, was the medium of choice to precipitate $[(Cu(hfa)_2)_2(4\text{-tpt})]_n$ (**1**), whose structure was determined by powder X-ray diffraction (PXRD) patterns by comparison to the simulated pattern (Figure 3a). Actually, TCE is a suitable solvent to carry out multiple synthetic procedures with particularly insoluble molecules; however, it is far from being considered a green solvent. Thus, a more sustainable route for reaching compound (**1**) was sought. The choice was to use green $scCO_2$ as a solvent, previously tested in the synthesis of other tritopic triazines.[25] By using this solvent, the target compound (**1**) could be precipitated, even PXRD analysis indicates that it was slightly tainted with a trace amount of a nonidentified product (Figure 3a).

Quite the reverse of (**1**), $[(Cu(hfa)_2)(4\text{-tpt})]_n$ (**2**) could not be directly precipitated from solution as a pure compound. The best results were obtained by precipitation in EtOEt. However, prolonged reaction times (>120 h) were needed, and the final product was contaminated with

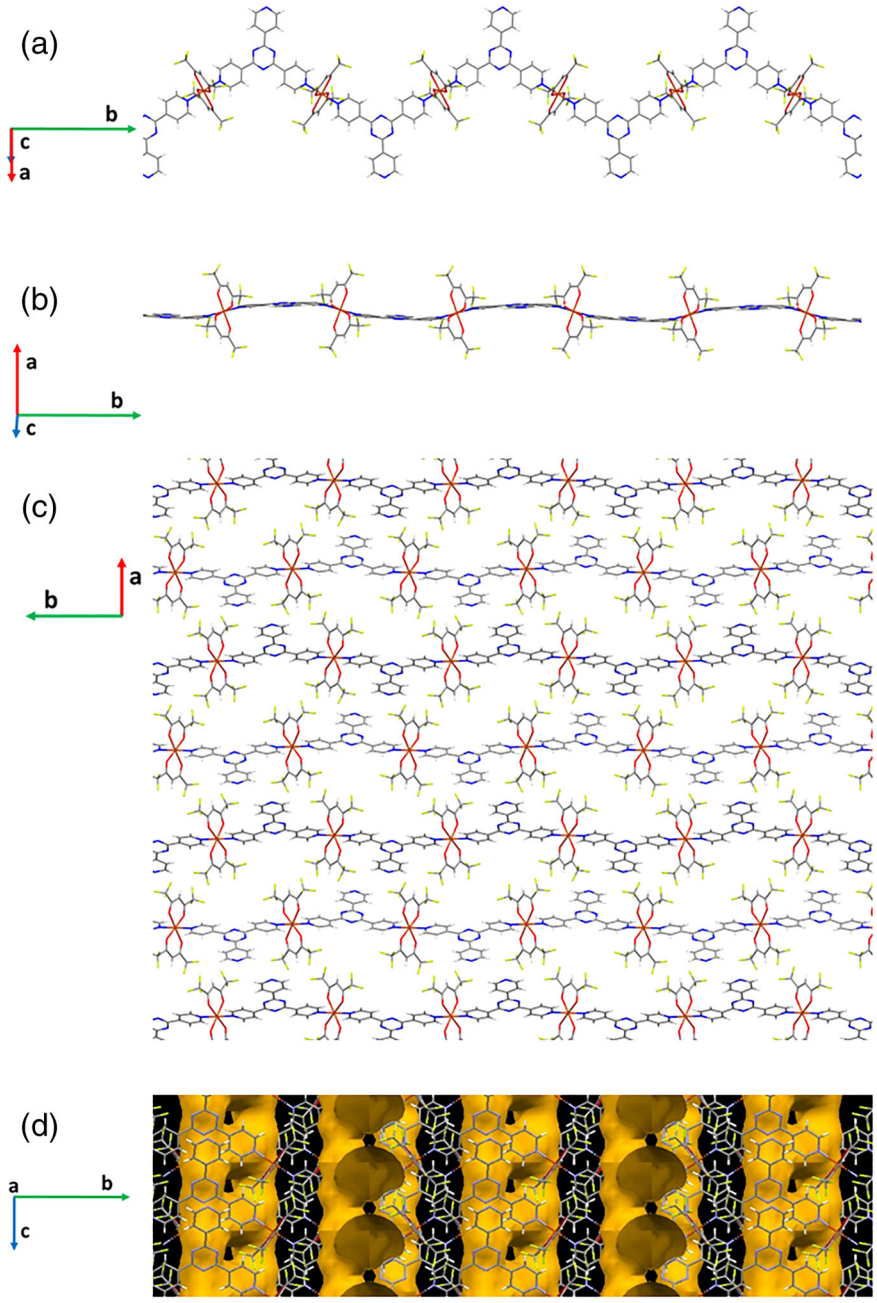

FIGURE 2 Crystal structure of $[(Cu(hfa)_2)(4\text{-tpt})]_n$ (**2**): (a,b) views of the chains with a different angle in respect to the 4-tpt linker, (c) packing view along ***c*** axis, showing the channels (these channels are occupied by water molecules, which are not shown for the clarity of the draw), and (d) void space analysis in the ***bc*** plane

linker excess. The best synthetic route for (**2**) was to go through the presence of an intermediate phase, either amorphous or crystalline, with an increased percentage of $Cu(hfa)_2$. The intermediate was then recrystallized in EtOEt, a nonpolar hard Lewis base solvent, which extracted $Cu(hfa)_2$ excess. Both compounds, (**1**) and (**2**), only differ in the amount of $Cu(hfa)_2$ units incorporated to the structure. Consequently, Fourier transformed infrared spectroscopy with attenuated total reflection accessory (FTIR-ATR) spectra denote great similarities between the two compounds (Figure S6). Elemental analysis agrees with the crystallographic composition elucidated for both compounds (see Section 4).

The phase transformation of (**1**) to (**2**) in EtOEt was qualitatively analyzed in this solvent. PXRD data indicated that the pattern of the sample obtained by treatment of compound (**1**) with this solvent math the one corresponding to compound (**2**) (Figure S7). EtOEt is a low polarity solvent; thus, in principle, it should not dissolve either compound (**1**) or (**2**). Actually, the dissolution of $[(Cu(hfa)_2)_2(4\text{-tpt})]_n$ was not visually observed, even after prolonged (24 h) treatment, because a solid was always present in the dispersion, but the analysis of the filtered solid indicates the formation of a new crystalline phase, $[(Cu(hfa)_2)(4\text{-tpt})]_n$, involving only approximately half of the $Cu(hfa)_2$ content, with an experimental

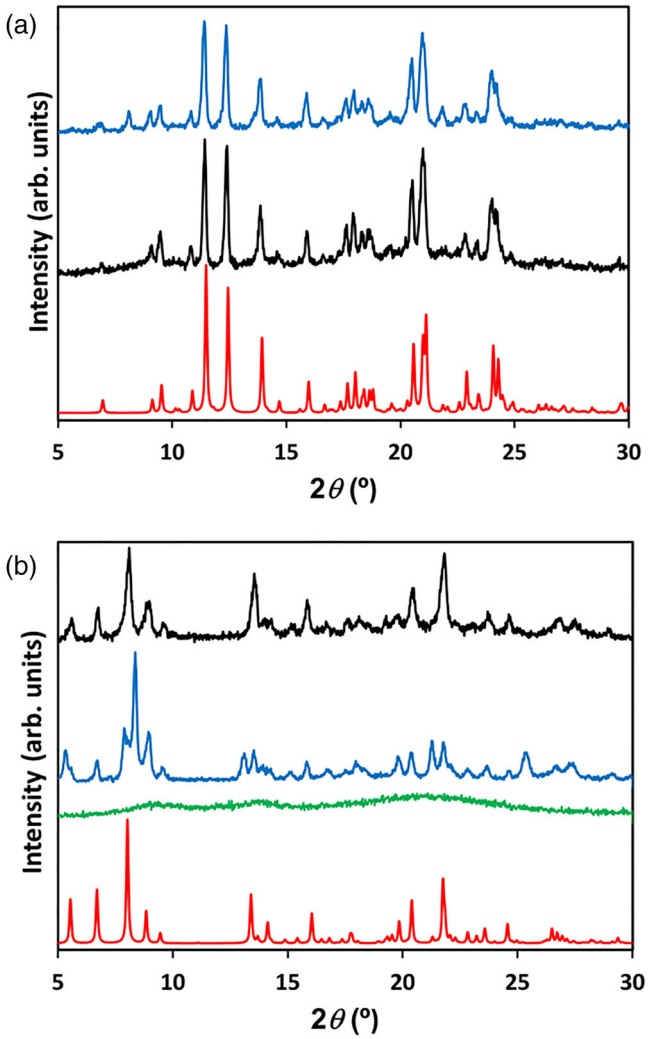

FIGURE 3 PXRD patterns of (a) $[(Cu(hfa)_2)_2(4\text{-tpt})]_n$ (**1**) simulated from single-crystal data (bottom, red line), precipitated in TCE (middle, black line) and precipitated in $scCO_2$ (up, blue line) in which * denotes peaks due to traces of unidentified impurity and (b) $[(Cu(hfa)_2)(4\text{-tpt})]_n$ (**2**) simulated from single-crystal data (bottom, red line), amorphous precipitate obtained in $CHCl_3$ (middle, green line), crystalline sample obtained after treatment of the amorphous sample with EtOEt (up, blue line), and sample obtained after activation under vacuum of the previous sample (up, black line)

Cu:4-tpt ratio of 1.15:1 according to elemental analysis. The analysis of several aliquots of the supernatant solution taken at different times during the 24 h treatment of $[(Cu(hfa)_2)_2(4\text{-tpt})]_n$ in EtOEt indicates the presence of only $Cu(hfa)_2$, with insignificant amounts of 4-tpt. These results are reasoned on the basis of a probable crystalline solid (**1**) → crystalline solid (**2**) (+$Cu(hfa)_2$ in solution) process. This transformation is facilitated by the relatively labile character of the $Cu(hfa)_2$ fragments linked to only one pyridine group in (**1**), which are solubilized in EtOEt and eliminated in (**2**) (Scheme 1). It is suggested that EtOEt solvent is not strong enough to break the bonds $Cu(hfa)_2$—4-tpt—$Cu(hfa)_2$. A crystalline solid (**1**) → solution ($Cu(hfa)_2$ + 4-tpt) → crystalline solid (**2**) process does not seems feasible in this case, mainly due to the almost null solubility of 4-tpt in this solvent. TGA characterization reveals a moderate thermal stability for both compounds, because they start to degrade at around 470–480 K in N_2 flow (Figure S8). A second-stage decomposition is observed at 540–550 K. The weight loss of compound (**1**) in the first step is more pronounced than for (**2**), indicating a larger amount of $[Cu(hfa)_2]$ units in the structure. For both materials, the by-products sublimated in the second step, thus giving a solid residue of almost zero.

An alternative route, consisting in the transformation of amorphous $[(Cu(hfa)_2)_2(4\text{-tpt})]$ → crystalline solid (**2**) (+$Cu(hfa)_2$ in solution), was designed to avoid the use of carcinogen TCE. Instead, $CHCl_3$ was used to precipitate the amorphous intermediate, which is further recrystallized in EtOEt. The different phases were analyzed by PXRD, and the patterns are shown in Figure 3b. The activation of the recrystallized solid under vacuum at 333 K induced a significant weight loss in the sample (4.40%), which clearly suggests that the material contains some residual solvent inside the voids evacuated during the degasification treatment. The material remains crystalline even after solvent elimination, although some small changes in the PXRD pattern were visible (Figure 3b), especially the fade of the peak at 2θ 8.34°. The pattern of the activated sample reasonably agrees with the simulated from the single-crystal structure.

2.4 | Adsorption properties

For compound (**1**), low temperature N_2 adsorption–desorption data indicate that the material behaves as a nonporous solid. Nevertheless, structural voids analysis performed with Mercury software detects noninterconnected pores (2.0%, probe radius 1.2 Å, Figure S9). For the activated compound (**2**), an isotherm corresponding to a microporous material was obtained (Figure 4a), with an apparent surface area of 190 $m^2\ g^{-1}$ and a micropore volume of 0.063 $cm^3\ g^{-1}$. After water elimination from the channels, void analysis performed with Mercury software detected a 13.9% void space. Hence, even both compounds have potential voids, only (**2**) displayed open pores, while the pores in (**1**) are blind. For compound (**2**), the adsorption of gasses was further analyzed at 273 K, choosing as probe molecules CO_2 and N_2. This MOF shows a noticeable CO_2 adsorption under the used experimental conditions and a clear preferential adsorption for CO_2 in front of N_2 (Figure 4b). The adsorption selectivity

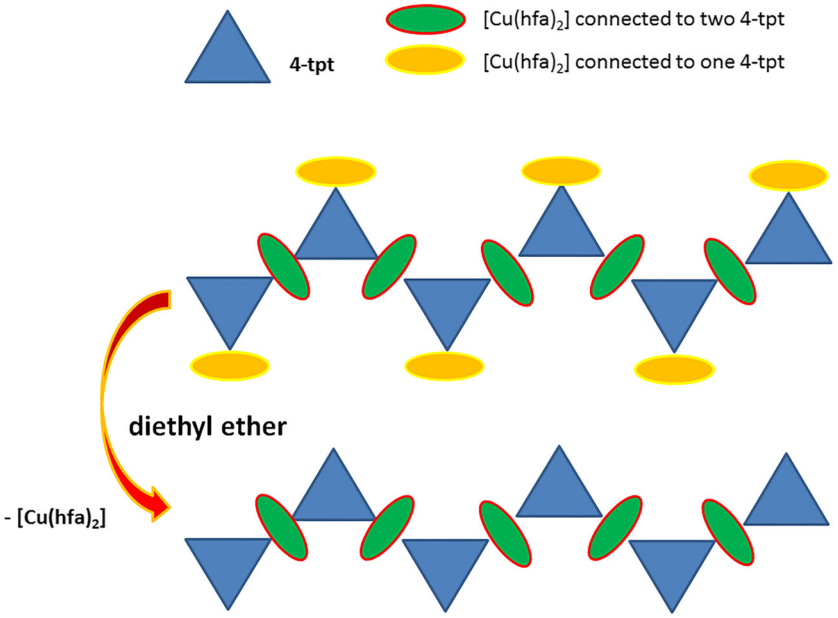

SCHEME 1 Proposed route to the transformation of (**1**) to (**2**) by the elimination in EtOEt of [Cu(hfa)$_2$] fragments bonded only to one 4-tpt linker

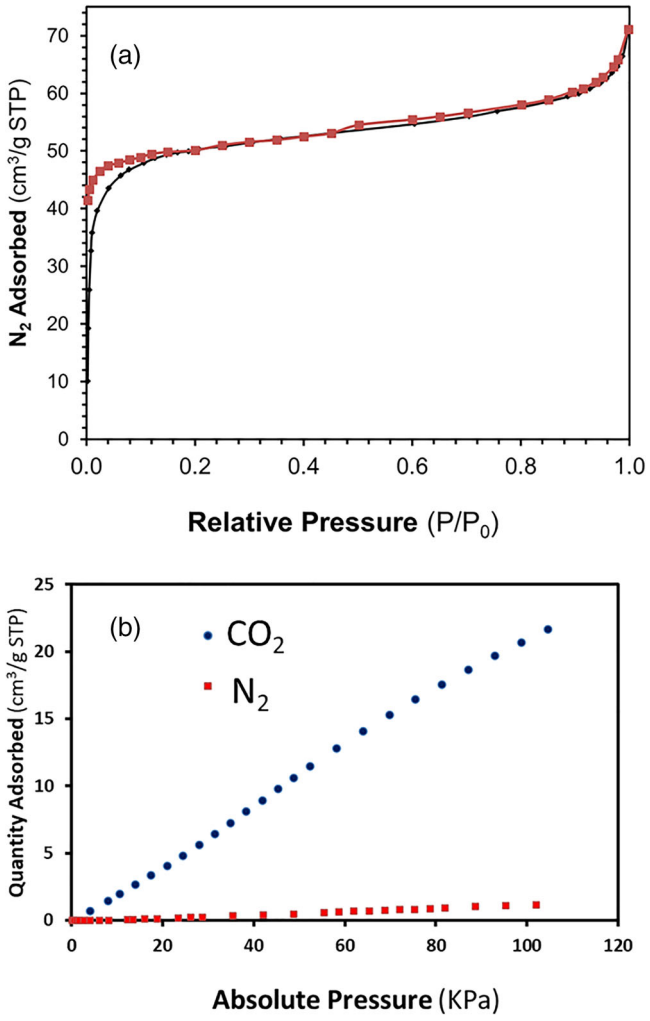

FIGURE 4 Gas adsorption measurements performed for compound [(Cu(hfa)$_2$)(4-tpt)]n (**2**): (a) adsorption isotherm of N_2 at 77 K and (b) adsorption of N_2 and CO_2 at 273 K

was preliminarily measured just from obtained CO_2 and N_2 uptakes, and given as the ratio percentage of the uptake, being of near 100% for CO_2. High CO_2 selectivity versus N_2 has been previously related to the presence of the triazine group in the crystalline structure of MOFs[15] and COFs.[33,34] In another recent report of a 4-tpt derived MOF, selectivity was related to a sieving effect.[35] The isosteric heats of adsorption (Q_{st}) for compound (**2**) were measured in this work as a function of CO_2 uptake (Figure S10). A constant Q_{st} value of -20 J mmol^{-1} was estimated, independently of the fractional adsorption coverage, thus indicating an energetically homogeneous adsorbent surface. The measured Q_{st} value, even being below of the energy corresponding to chemical bond formation, is quite high due to the presence of triazine rings provoking strong physical adsorption of CO_2 molecules on the pore walls of (**2**). Nevertheless, the Q_{st} can be considered moderated enough to favor regeneration.

3 | CONCLUSIONS

This study demonstrates that even with topological symmetric linkers, such as the 4-tpt molecule, which do not have alternative conformations, different MOFs can be obtained, starting from the same reagents, by manipulating the composition and the structure through the used solvent. Specifically, the same metal–ligand combination, for example, Cu(hfa)$_2$ and 4-tpt, led to two MOFs different in composition and structure: $[(Cu(hfa)_2)_2(4\text{-tpt})]_n$ (**1**) and $[(Cu(hfa)_2)(4\text{-tpt})]_n$ (**2**), with a 2:1 and 1:1 Cu(II):4-tpt ratio, respectively. This is a clear example of the possibility of having different topologies in symmetric

linker MOFs, just obtained by employing different synthetic solvents. It is demonstrated that the solvent used in the synthesis can determine the denticity (tritopic or ditopic) of the 4-tpt in their combination with $[Cu(hfa)_2]$. Moreover, the proper choice of solvent allows the probable solid-to-solid transformation of (**1**) to (**2**). Both compounds are 1D MOFs, although only compound (**2**) has an open porous structure that can be accessed by small gas molecules, such as N_2 or CO_2, which make this compound a potential candidate for gas adsorption and separation. Particularly, it shows a high adsorption capacity for CO_2 at 273 K and a low partial pressure of the gas, comparable with that of standard Zeolita X13. The enhanced adsorption is related to the presence of exposed and noncoordinated N in the triazine rings of the linker.

4 | EXPERIMENTAL SECTION

4.1 | Materials

Precursor reagents $Cu(hfa)_2{\cdot}xH_2O$ (Aldrich, 94.4% $Cu(hfa)_2$ according to certificate of analysis, abbreviated $Cu(hfa)_2$ throughout the text), 2,4,6-tris(4-pyridyl)-1,3,5-triazine (4-tpt), and solvents 1,1,2-TCE, diethyl ether, chloroform ($CHCl_3$), ethanol (EtOH, absolute), and compressed CO_2 (99.95%) were purchased from commercial sources and used as received.

4.2 | Synthesis

4.2.1 | Synthesis of $[(Cu(hfa)_2)_2(4\text{-tpt})]_n$ (**1**)

Route A: 4-tpt (100.0 mg, 0.320 mmol) and $Cu(hfa)_2{\cdot}xH_2O$ (325 mg, 0.642 mmol) were dissolved in hot TCE (353 K, 80 ml), and the resulting green solution was allowed to cool down, thus giving a crystalline green precipitate that was filtered and cleaned with cold TCE, and finally dried under vacuum at 333 K. Yield ~80 wt%. Anal. calc. for $C_{38}H_{16}O_8N_6F_{24}Cu_2$ (1267.7 g mol^{-1}): C, 36.01; H, 1.27; N, 6.63. Found: C, 36.31; H, 1.03; N, 6.89%. **Route B:** reactions in $scCO_2$ were performed in a 5 ml Pyrex vial placed into a 100 ml high pressure autoclave with two opposite sapphire windows (TharDesign). The vial was charged with $Cu(hfa)_2{\cdot}H_2O$ (208 mg, 0.411 mmol) and 4-tpt (64.0 mg, 0.205 mmol) organic linker. A small magnetic bar was also added, and the vial was finally capped with cellulose filter paper. Experiments were performed at 20 MPa and 333 K. The vial was stirred at 500 rpm. After a running period of 20 h, the product was washed with fresh $scCO_2$ twice to eliminate any possible residue. The autoclave was then depressurized and cooled down to room temperature to recover a green powder.

4.2.2 | Synthesis of $[(Cu(hfa)_2)(4\text{-tpt})]_n$ (**2**)

A solution of 4-tpt (50.0 mg, 0.160 mmol) and $Cu(hfa)_2{\cdot}H_2O$ (85 mg, 0.168 mmol) in $CHCl_3$ was evaporated to dryness yielding an amorphous residue. Then, the solid was suspended in EtOEt and stirred during 48 h. During this period, $Cu(hfa)_2$ excess solubilized. The resulting crystalline solid was filtrated and washed with EtOEt twice. Samples were dried under vacuum at 333 K. Yield ~90%, respect to 4-tpt. Anal. calc. for $C_{28}H_{14}O_8N_6F_{12}Cu$ (790.0 mol^{-1}): C, 42.57; H, 1.79; N, 10.64. Found: C, 42.76; H, 1.65; N, 10.57%.

4.3 | Characterization methods

Samples chemical composition was assessed by elemental analysis (E.A., Thermo Carlo Erba Flash 2000). PXRD patterns were recorded at room temperature in a Siemens D5000 diffractometer, using the Cu Kα incident radiation. Fourier transformed infrared spectroscopy (FTIR) spectra were recorded on a Tensor 27 (Bruker) spectrometer, equipped with an attenuated total reflection (ATR) accessory model MKII Golden Gate with a diamond window in the range 4000–600 cm^{-1}. The textural properties were determined by N_2 adsorption/desorption at 77 K using an ASAP 2020 Micromeritics Inc. equipment. The micropore apparent surface area and pore volume were determined by the *t* method. For both, elemental analysis and textural characterization, the samples were first degassed at 333 K during 24 h to eliminate adsorbed solvent molecules. The same equipment was used to measure the volumetric gas adsorption of N_2 and CO_2 at 273 K. The isosteric heat of adsorption (Q_{st}) was calculated from the CO_2 isotherms measured at 273, 298, and 313 K by using the Clausius−Clapeyron equation. Thermogravimetric analysis (TGA, NETZSCH-STA 449 F1 Jupiter) was performed under a N_2 atmosphere increasing the temperature in steps of 10 K min^{-1} up to 1123 K.

4.4 | Crystal structures

Synchrotron X-ray powder diffraction (SR-XRPD) data for compound (**1**) were collected at the high-resolution station of the MSPD beamline (BL04) at ALBA synchrotron.[36] The sample was introduced in a 0.7 mm glass capillary and measured (10 min) in transmission at an energy of 25 keV (0.49587 Å wavelength, determined

with a Si NIST-640d reference) using the Mythen-II detector (six modules, 1280 channels/module, 50 μm/channel, sample-to-detector distance 550 mm) at room temperature. The diffraction pattern was indexed using DICVOL04,[37] and the intensities extracted with DAjust software[38] were used in the direct-space solution program TALP[39] to obtain a crystal structure that was finally refined with the Rietveld refinement program RIBOLS.[40] The values for the interatomic distance restraints and angles were taken from MOGUL.[41] The crystallographic data and refinement details for compound (**1**) are summarized in Table S1 of the SI. Rietveld refinement plot is shown in Figure S11.

For compound (**2**), single-crystal X-ray diffraction (SCXRD) experiments were performed in the XALOC beamline at ALBA synchrotron (Spain).[42] Data were collected at 100 K with a 0.72932 Å wavelength using the Dectris Pilatus 6 M detector placed at 120 mm from the sample. The ϕ scans were performed from 0° to 360° in steps of 0.5° with a collection time of 0.15 step^{-1}. The scan was repeated at three different κ angles (0°, 45°, and 90°) and merged afterwards to increase the completeness and redundancy when possible. Data were indexed, integrated, and scaled using the XDS software.[43] The crystal structure was solved by intrinsic phasing and refined with SHELXL (version 2014/7)[44] using Olex2 as graphical interface.[45] Crystallographic data are summarized in Table S2.

CCDC 2164405 (**1**) and 2164404 (**2**) contain the supplementary crystallographic data for this paper. These data can be obtained free of charge via www.ccdc.cam.ac.uk/data_request/cif.

ACKNOWLEDGMENTS

This work was supported by the Spanish Ministry of Science and Innovation (MICINN) through the Severo Ochoa Program for Centers of Excellence (CEX2019-000917-S) and the Spanish National Plan of Research with project PID2020-115631GB-I00. The measures for the elucidation of the crystal structures were performed at MSPD and XALOC beamlines at ALBA Synchrotron with the collaboration of ALBA staff.

AUTHOR CONTRIBUTIONS

Núria Portolés-Gil: Formal analysis; investigation; methodology. **Oriol Vallcorba:** Data curation; formal analysis; investigation; methodology. **Julio Fraile-Sainz:** Formal analysis; methodology. **Ana M. López-Periago:** Formal analysis; methodology. **Concepción Domingo:** Investigation; project administration; resources; supervision; writing-review and editing. **José A. Ayllón:** Conceptualization; formal analysis; investigation; methodology; supervision; writing-original draft; writing-review and editing.

DATA AVAILABILITY STATEMENT

The data that supports the findings of this study are available in the Supporting Information of this article.

ORCID

Núria Portolés-Gil https://orcid.org/0000-0002-2580-4641
Oriol Vallcorba https://orcid.org/0000-0001-6499-7688
Julio Fraile-Sainz https://orcid.org/0000-0003-2961-7920
Ana M. López-Periago https://orcid.org/0000-0002-3777-3205
Concepción Domingo https://orcid.org/0000-0002-6976-8283
José A. Ayllón https://orcid.org/0000-0001-7965-7424

REFERENCES

[1] S. Kitagawa, *Acc. Chem. Res.* **2017**, *50*, 514.
[2] Q. Wang, D. Astruc, *Chem. Rev.* **2020**, *120*, 1438.
[3] B. Therrien, *J. Organomet. Chem.* **2011**, *696*, 637.
[4] T. J. Podesta, A. G. Orpen, *Cryst. Growth Des.* **2005**, *5*, 681.
[5] L. A. Barrios, J. Ribas, G. Aromí, J. Ribas-Ariño, P. Gamez, O. Roubeau, S. J. Teat, *Inorg. Chem.* **2007**, *46*, 7154.
[6] H. L. Chen, M.-X. Li, X. He, Z.-X. Wang, M. Shao, S.-R. Zhu, *Inorg. Chim. Acta* **2010**, *363*, 3186.
[7] G. Brunet, D. A. Safin, I. Korobkov, A. Cognigni, M. Murugesu, *Cryst. Growth des.* **2016**, *16*, 4043.
[8] R. A. Polunin, N. P. Burkovskaya, S. V. Kolotilov, M. A. Kiskin, A. S. Bogomyakov, S. A. Sotnik, I. L. Eremenko, *Russ. Chem. Bull.* **2014**, *63*, 252.
[9] S. R. Batten, B. F. Hoskins, B. Moubaraki, K. S. Murray, R. Robson, *Chem. Commun.* **2000**, 1095.
[10] Y. Zhao, L. Li, Z.-Y. Liu, B. Ding, X.-G. Wang, Y. Luo, X.-J. Zhao, E.-C. Yang, *Cryst. Growth Des.* **2021**, *21*, 1218.
[11] S. A. Sotnik, R. A. Polunin, M. A. Kiskin, A. M. Kirillov, V. N. Dorofeeva, K. S. Gavrilenko, I. L. Eremenko, V. M. Novotortsev, S. V. Kolotilov, *Inorg. Chem.* **2015**, *54*, 5169.
[12] A. Polunin, N. P. Burkovskaya, J. A. Satska, S. V. Kolotilov, M. A. Kiskin, G. G. Aleksandrov, O. Cador, L. Ouahab, I. L. Eremenko, V. V. Pavlishchuk, *Inorg. Chem.* **2015**, *54*, 5232.
[13] Y.-Y. Zhang, Q. Liu, L.-Y. Zhang, Y.-M. Bao, J.-Y. Tan, N. Zhang, J.-Y. Zhang, Z.-J. Liu, *Dalton Trans.* **2021**, *50*, 647.
[14] W. J. Gee, L. E. Hatcher, C. A. Cameron, C. Stubbs, M. R. Warren, A. D. Burrows, P. R. Raithby, *Inorg. Chem.* **2018**, *57*, 4959.
[15] T. R. Ramadhar, S.-L. Zheng, Y.-S. Chen, J. Clardy, *CrstEngComm* **2017**, *19*, 4528.
[16] Y. Inokuma, S. Yoshioka, J. Ariyoshi, T. Arai, Y. Hitora, K. Takada, S. Matsunaga, K. Rissanen, M. Fujita, *Nature* **2013**, *495*, 461.
[17] H.-M. Wen, B. Li, L. Li, R.-B. Lin, W. Zhou, G. Qian, B. Chen, *Adv. Mater.* **2018**, *30*, 1704792.
[18] Y. Belmabkhout, V. Guillerm, M. Eddaoudi, *Chem. Eng. J.* **2016**, *296*, 386.
[19] H. He, Q. Sun, W. Gao, J. A. Perman, F. Sun, G. Zhu, B. Aguila, K. Forrest, B. Space, S. Ma, *Angew. Chem. Int. Ed.* **2018**, *130*, 4657.

[20] K. D. Vogiatzis, A. Mavrandonakis, W. Klopper, G. E. Froudakis, *ChemPhysChem* **2009**, *10*, 374.
[21] X. Wang, M. Chen, M. Du, *Inorg. Chem.* **2016**, *55*, 6352.
[22] G. I. Dzhardimalieva, I. E. Uflyand, *RSC Adv.* **2017**, *7*, 42242.
[23] N. Portolés-Gil, S. Gowing, O. Vallcorba, C. Domingo, A. M. López-Periago, J. A. Ayllón, *J. CO2 Util.* **2018**, *24*, 444.
[24] N. Portolés-Gil, S. Gómez-Coca, O. Vallcorba, G. Marbán, N. Aliaga-Alcalde, A. López-Periago, J. A. Ayllón, C. Domingo, *RSC Adv.* **2020**, *10*, 45090.
[25] N. Portolés-Gil, A. M. López-Periago, A. Borrás, J. Fraile, E. Solano, O. Vallcorba, J. G. Planas, J. A. Ayllón, C. Domingo, *Cryst. Growth Des.* **2020**, *20*, 3304.
[26] M.-X. Li, Z.-X. Miao, M. Shao, S.-W. Liang, S.-R. Zhu, *Inorg. Chem.* **2008**, *47*(11), 4481.
[27] S. M. Neville, G. J. Halder, K. S. Murray, B. Moubaraki, C. J. Kepert, *Aust. J. Chem.* **2013**, *66*, 452.
[28] Y. Ishimaru, M. Kitano, H. Kumada, N. Koga, H. Iwamura, *Inorg. Chem.* **1998**, *37*, 2273.
[29] D. Gatteschi, J. Laugier, P. Rey, C. Zanchini, *Inorg. Chem.* **1987**, *26*, 938.
[30] S. Winter, E. Weber, L. Eriksson, I. Csöregh, *New J. Chem.* **2006**, *30*, 1808.
[31] P. Larpent, A. Jouaiti, N. Kyritsakas, M. W. Hosseini, *Dalton Trans.* **2014**, *43*, 2000.
[32] A. Ota, L. Ouahab, S. Golhen, O. Cador, Y. Yoshida, G. Saito, *New J. Chem.* **2005**, *29*, 1135.
[33] Y. Zeng, R. Zou, Y. Zhao, *Adv. Mater.* **2016**, *28*, 2855.
[34] S. K. Kundu, A. Bhaumik, *ACS Sustainable Chem. Eng.* **2016**, *4*, 3697.
[35] B.-B. Qian, P.-C. Song, H.-X. Nie, B. Zhang, J.-Y. Zheng, M.-H. Yu, Z. Chang, *Dalton Trans.* **2021**, *50*, 5244.
[36] F. Fauth, I. Peral, C. Popescu, M. Knapp, *Powder Diffraction.* **2013**, *28*(S2), S360.
[37] A. Boultif, D. Louer, *J. Appl. Cryst.* **2004**, *37*, 724.
[38] O. Vallcorba, J. Rius, C. Frontera, I. Peral, C. Miravitlles, *J. Appl. Cryst.* **2012**, *45*, 844.
[39] O. Vallcorba, J. Rius, C. Frontera, C. Miravitlles, *J. Appl. Cryst.* **2012**, *45*, 1270.
[40] J. Rius, O. Vallcorba, **2012**. https://crystallography.icmab.es/software.
[41] I. J. Bruno, J. C. Cole, M. Kessler, J. Luo, W. D. S. Motherwell, L. H. Purkis, B. R. Smith, R. Taylor, R. I. Cooper, S. E. Harris, A. G. Orpen, *J. Chem. Inf. Comput. Sci.* **2004**, *44*, 2133.
[42] J. Juanhuix, F. Gil-Ortiz, G. Cuní, C. Colldelram, J. Nicolás, J. Lidón, E. Boter, C. Ruget, S. Ferrer, J. Benach, *J. Synchrotron Radiat.* **2014**, *21*, 679.
[43] W. Kabsch, *Acta Crystallogr.* **2010**, *D66*, 125.
[44] G. M. Sheldrick, *Acta Crystallogr.* **2015**, *C71*, 3.
[45] O. V. Dolomanov, L. J. Bourhis, R. J. Gildea, J. A. K. Howard, H. Puschmann, *J. Appl. Cryst.* **2009**, *42*, 339.

SUPPORTING INFORMATION

Additional supporting information can be found online in the Supporting Information section at the end of this article.

How to cite this article: N. Portolés-Gil, O. Vallcorba, J. Fraile-Sainz, A. M. López-Periago, C. Domingo, J. A. Ayllón, *Appl Organomet Chem* **2023**, *37*(1), e6930. https://doi.org/10.1002/aoc.6930